

The bending-kinking analysis of a single-walled carbon nanotube—a combined molecular dynamics and continuum mechanics technique

K. MYLVAGANAM, T. VODENITCHAROVA, L. C. ZHANG*

School of Aerospace, Mechanical and Mechatronic Engineering, The University of Sydney, NSW, 2006, Australia

E-mail: zhang@aeromech.usyd.edu.au

Published online: 12 April 2006

This paper investigates the deformation mechanism of a single-walled carbon nanotube in pure bending. The molecular dynamics analysis and continuum mechanics characterisation were used together to achieve a deeper understanding. It was found that at a bending angle of 24° the nanotube buckles locally, forming a kink in the middle of the nanotube. As the bending angle increases, the kink progresses along the nanotube and varies its shape in both longitudinal and circumferential directions. The kink formation can be considered as the result of rotations of planes/surfaces about the moving and stationary hinge lines. It was also found that the kink deformation influences the load bearing capacity of the nanotube.

© 2006 Springer Science + Business Media, Inc.

1. Introduction

The high flexibility of single-walled carbon nanotubes (SWNTs) has been extensively studied for most of the generic types of loading. Reports show that SWNTs possess exceptionally large fracture resistance and can undergo reversible deformation to very high strain levels. It has been shown [1] that the buckling in bending can facilitate the reactivity of nanotubes that will be useful in designing schemes for molecular devices including contact to surfaces and interconnects. Both experiments and molecular dynamics simulations have shown that carbon nanotubes (CNTs) can be bent through large angles without failure.

Experimentally, the bent CNTs were observed using the high resolution electron microscope (HREM) and atomic force microscope (AFM) imaging techniques. Iijima *et al.* [2] reported the bending of SWNTs and multi-walled nanotubes (MWNTs) using HREM observations in which the deformations were introduced during handling such as collecting them from the chamber and transferring them to the electron microscope. Postma *et al.* [3] demonstrated the buckling and bending of CNTs using the AFM tip manipulation technique, and observed that the CNTs underwent elastic deformation. Falvo *et al.* [4] bent MWNTs through large angles using the tip of an AFM without undergoing catastrophic failure.

Theoretically, the bending of CNTs has been studied by molecular dynamics (MD) simulations [2]. At a critical bending angle, the compressive wall in the middle of the SWNTs displaced inwards and formed a single V-shaped kink. It was reported that the top and bottom walls of the nanotube could not get closer than 3.5\AA even at a very large angle because at that distance the van der Waals interaction between the walls became strongly repulsive. Buckling was found to be elastic up to a bending angle of 110° , after which the atomic bonds broke and the nanotube failed.

A similar analysis was conducted by Yakobson *et al.* [5] and it was suggested that the behaviour of CNTs could be studied by continuum mechanics as a cheaper alternative to the time-consuming (MD) simulations. A model for the bending of a SWNT was consequently developed by Vodenitcharova and Zhang [6]. The response of a SWNT was studied separately for the pre-buckling stage, the onset of local buckling, and the kink development up to a moderate bending angle.

The present paper combines the MD simulation technique [7], which offers discrete displacements at individual atoms, and continuum mechanics analysis, which mimic the atomistic deformation to a continuum framework, to examine the deformation mechanism

*Author to whom all correspondence should be addressed.

and bending capacity of a SWNT at small to moderate bending angles.

2. Computational technique

A straight open zigzag SWNT of length $L = 75.3\text{\AA}$ and radius $R = 6.65\text{\AA}$ was bent by rotating its end sections step-wisely. A classical MD method was used. The interatomic interactions were described by reactive bond-order hydrocarbon potential formulated by Brenner [8, 9], which has been successfully used to simulate the deformation of CNTs. Mylvaganam and Zhang [7] pointed out that in order to minimize the heat conduction problem and to improve the computational efficiency, the Berendsen thermostat should be applied to all atoms except those being rigidly held. The simulations were carried out at 300 K with a time step of 0.5 fs. Ten rings of atoms on each end of the CNT were rotated out of plane in steps of 2° . In each step, these atoms were held rigid at their rotated positions and the rest were relaxed to a minimum energy using the conjugate gradient algorithm. Then, those relaxed atoms were held at their new positions and the end atoms that were held rigidly in the previous step were relaxed to the minimum energy. This procedure was repeated up to a bending angle of 64° . The strain energy due to bending was calculated as the difference in the total energy of the bend tube and the initial energy of the straight tube.

3. Molecular dynamics analysis

Bending along the nanotube was smooth at small bending angles. The tube experienced simple compression on the inner side and tension on the outer side. Initially the strain energy increased quadratically with the bending angle. At around 24° , the nanotube buckled in the middle and a kink developed on the inner side. As a result of the release of the compressive stress, the strain energy of the nanotube dropped. On further bending, the kink pronounced and the strain energy increased almost linearly with the bending angle as shown in Fig. 1.

The mechanism of kink formation and its development was analysed and presented in the following sections.

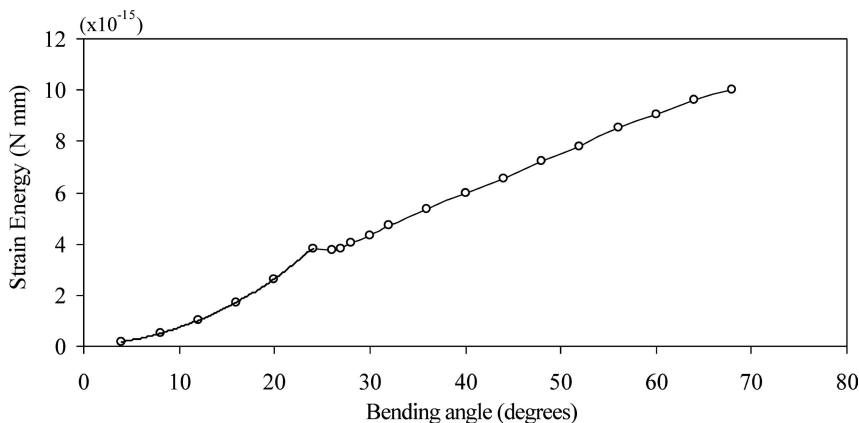


Figure 1 Strain energy vs. bending angle of a SWNT in pure bending.

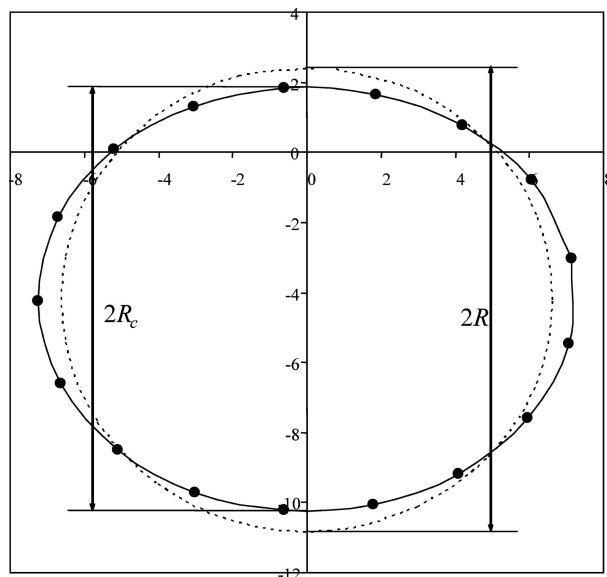


Figure 2 Original (dotted line) and deformed (line with solid circles, where the circles represent the atoms) cross sections of the SWNT at a bending angle of $\psi = 20^\circ$ (dimensions are in \AA).

It was observed that small bending angles ψ only flatten the SWNT symmetrically about planes $\theta = 0^\circ$ and 90° as the initially-circular cross sections becomes oval. This ovalisation is uniform along the nanotube since the end sections are left free to move in their planes. The degree of flattening can be conventionally measured by the flattening ratio [10], $\zeta = (R - R_c)/R$, where R_c is the current half-distance between the extreme top and bottom points of the cross-section. For small ψ , R_c is small and hence ζ is small. For example, at $\psi = 20^\circ$ (Fig. 2), ζ is calculated as 0.10. ζ increases for larger bending angles.

As ψ increases, a point is reached at which the inner wall of the SWNT suddenly buckles and moves inwards, thus forming a kink in the middle of the nanotube (Fig. 3a). In the MD simulation this takes place around $\psi = 24^\circ$. The occurrence of the kink changes the deformed shape of the cross sections along the nanotube axis, as can be seen in Fig. 3b at a bending angle of $\psi = 28^\circ$. The end cross sections of the nanotube rotate as rigid at an angle of $\psi/2$.

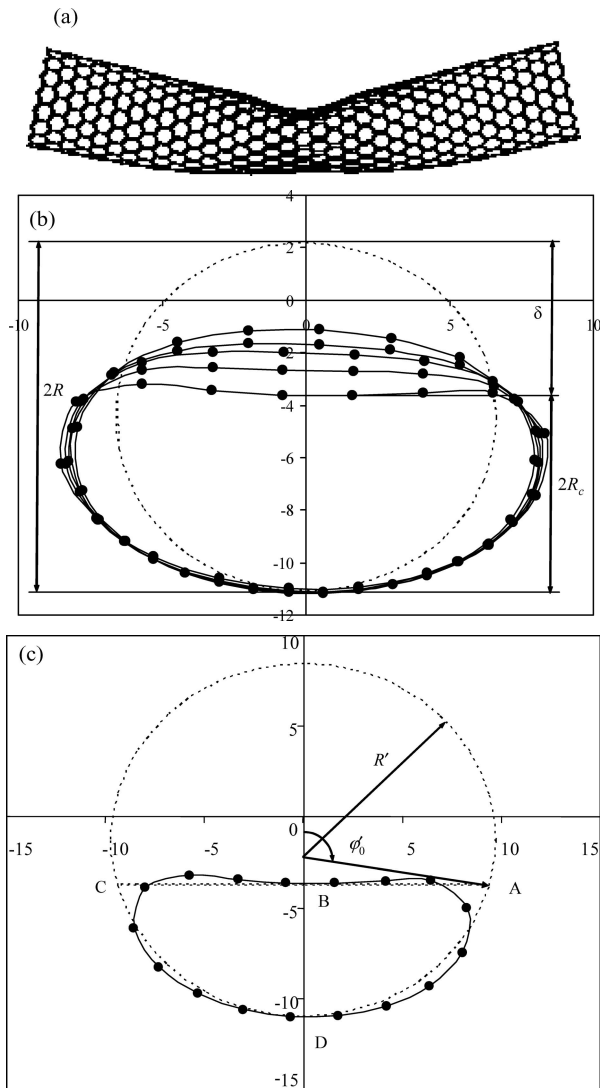


Figure 3 (a) Longitudinal section of the SWNT once the kink is formed. (b) Cross-sectional view of the deformed atomic rings at a bending angle of $\psi = 28^\circ$ (the dotted line is the original cross section and the lines with solid circles correspond to various deformed cross sections along the SWNT axis, where the solid circles represent the atoms). (c) Cross-sectional view (line with solid circles, where the solid circles represent the atoms) in the middle of the kink at $\psi = 28^\circ$, and the approximate model (dotted line) consisting of a top flat part ABC and a bottom arc ADC having $R' = 9.75\text{\AA}$.

This angle of rotation decreases towards the middle of the kink, where it becomes zero. Three different deformation shapes of the cross section can be distinguished along the nanotube axis. While at the ends of the beam, the cross sections remain almost circular, midway between the ends and the middle of the nanotube they start flattening, though remaining planar. At a distance of $3.8R$ from the middle of the kink the flattening ratio ζ is around 0.04, at a distance of $3.5R$ it is about 0.098, and at a distance of R , $\zeta = 0.24$. At a distance from the middle of the kink shorter than R , the top parts of the cross sections flatten more than the bottom parts, they become flat and even concave; however the cross sections still remain almost planar.

A closer look at the longitudinal section of the SWNT at $\psi = 28^\circ$ reveals that the kink starts at a distance

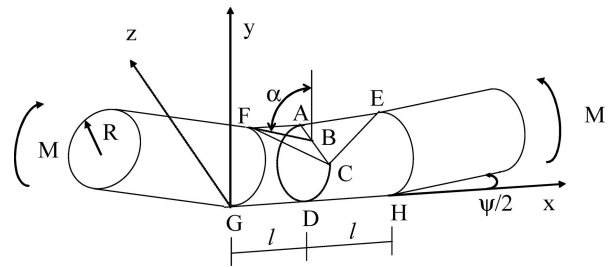


Figure 4 Schematic representation of the kink under bending.

$l = R$ from the middle of the nanotube. In the middle of the kink the flattening ratio is $\zeta = 0.355$ and the drop of the cross section $\delta = 2(R - R_c)$ (Fig. 3b) appears to be around $0.89R$. It can also be seen that the cross sections at different locations along the kink have almost the same circumferential curvature in their bottom arc parts, but their sides bulge more towards the middle of the kink. Moreover, it can be concluded by observation that during kinking the perimeter of the cross sections does not change; the cross sections only bend. Similar is the conclusion for the kinking of the SWNT in the longitudinal direction, i.e., the length of the SWNT remains almost unchanged. Therefore the kinking phenomenon in pure bending is in-extensional.

The shape of the deformed cross section of the kink can be presented in a simplified form, consisting of a straight line AC on the top of the kink and a circular arc of radius R' at the bottom (Fig. 3c); obviously AC and R' vary along the kink. Apparently the length of AC decreases almost linearly from the middle of the kink towards its ends, where it becomes zero. Points A and C can be seen as positioned on a stationary hinge line AC, as well as on hinge lines AE, CE, AF and CF (Fig. 4), moving as ψ increases. From the MD results the parameters of the idealised cross sections were estimated to be $y_B = DB = 7.34\text{\AA}$, $\delta = 6.03\text{\AA}$, $AC = 17.67\text{\AA}$, $R' = 9.75\text{\AA}$ and $\varphi'_0 = 101^\circ$ (see Fig. 3c for the definition of φ'_0).

The simplified shape of the kink consists of top triangular plates ABCF and ABCE, and bottom circular parts ADCGF and ADCHE (Fig. 4). This model has been applied to the present SWNT with the Poisson's ratio $\mu = 0.19$, Young modulus $E = 4.88$ TPa and thickness of the nanotube wall $t = 0.617\text{\AA}$ [11]. It follows that the onset of buckling occurs at $\psi = 23.3^\circ$, which is practically the same angle at kinking provided by the MD simulations presented above. At $\psi = 28^\circ$, the mechanics model leads to $l = R$, $y_B = DB = 7.22\text{\AA}$, $\delta = 6.099\text{\AA}$, $AC = 17.35\text{\AA}$, $R' = 8.82\text{\AA}$ and $\varphi'_0 = 100.5^\circ$, i.e., virtually the same results as the MD findings. It can therefore be concluded that the Vodenitcharova-Zhang's continuum model [6] gives reasonable prediction for small to medium angles.

4. Mechanics analysis

The bending moments in the walls of the kink and the moment-bearing capacity of the SWNT, considered as

continuum, can be estimated for a given angle ψ from the displacements of the atoms. Let the coordinates of the atoms are measured in a coordinate system XYZ set in the middle cross section of the SWNT (Figs. 5a and b), and let X_0 , Y_0 and Z_0 be the original coordinates before deformation and X' , Y' and Z' be the coordinates after deformation. The radius-vector of an atom is the sum of its original radius vector, its displacement as a rigid body, and its displacement vector $\mathbf{u} + \mathbf{v} + \mathbf{w}$ due to straining of the SWNT, where \mathbf{u} , \mathbf{v} and \mathbf{w} are the displacements in the longitudinal, circumferential and radial direction, respectively. One can avoid considering the rigid body translation and rotation by setting a new coordinate system $X'Y'Z'$ at the bottom point M'_b of a particular atomic ring, and rotate it at an angle γ , in order to rest in the plane of the deformed cross section (Figs. 5a and b). Then, the deformation of the atom is expressed in terms of \mathbf{v} and \mathbf{w} only, measured from the original location of the undeformed circle in the coordinate system $X'Y'Z'$. The geometrical relations between the magnitudes of the two displacements, i.e., w and v , and the current coordinates of the atom are as follows (see Fig. 5b)

$$\begin{aligned} X' &= X_0 - w \cos \theta - v \sin \theta \\ Y' &= Y_0 - w \sin \theta + v \cos \theta. \end{aligned} \quad (1)$$

Solving for w and v , Equation 1 yields

$$\begin{aligned} w &= -(Y' - Y_0) \sin \theta - (X' - X_0) \cos \theta \\ v &= (Y' - Y_0) \cos \theta - (X' - X_0) \sin \theta. \end{aligned} \quad (2)$$

Knowing w and v , one can estimate the cross-sectional circumferential curvature $k_{\theta\theta}$ and the bending moments in the circumferential direction $M_{\theta\theta}$ of the SWNT, as well as the curvature k_{zz} and bending moment M_{zz} in the longitudinal direction [10]

$$\begin{aligned} k_{\theta\theta} &= -\frac{1}{R^2} \left(\frac{\partial^2 w}{\partial z^2} + w \right), \\ M_{\theta\theta} &= -D [\mu k_{zz} + k_{\theta\theta}] \\ k_{zz} &= -\frac{\partial^2 w}{\partial z^2} \\ M_{zz} &= -D [k_{zz} + \mu k_{\theta\theta}], \end{aligned} \quad (3)$$

where $D = \frac{Et^3}{12(1-\mu^2)}$ is the bending stiffness of the continuum SWNT. The terms containing μ have a negligible contribution to the bending moments in Equation 3, so that the graphs of $M_{\theta\theta}$ and M_{zz} resemble those of $k_{\theta\theta}$ and k_{zz} , respectively; the difference is a multiplying factor, i.e., the bending stiffness D .

The formulae in Equation 1–3 can be applied to the displacements of the atoms obtained by MD. Figs. 6a and b show the distribution of $k_{\theta\theta}$ and $M_{\theta\theta}$ at two specific locations along the kink, at a given bending angle $\psi = 28^\circ$. The kink starts at a distance of R from the middle of the kink, where the cross section is oval

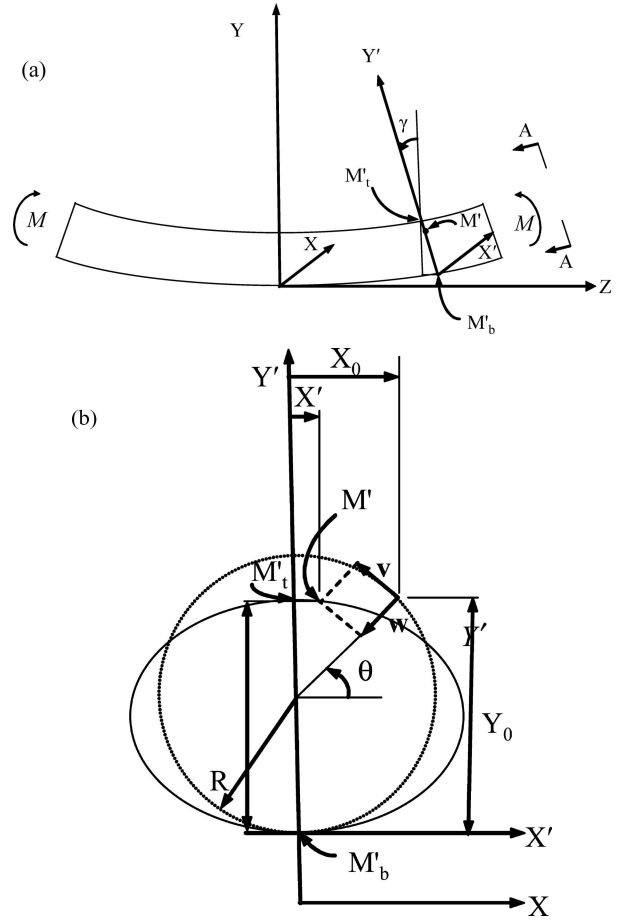


Figure 5 (a) Coordinate systems for the calculation of the displacements in a SWNT in bending; (b) Section A-A of (a) and the original circular cross section (dotted line).

(Fig. 6a), and bends more towards the middle of the kink as both the circumferential curvature and the circumferential bending moment increase. For example, at a distance of $0.64R$ from the middle of the kink, where the top part of the cross section is almost flat, $k_{\theta\theta}$ and $M_{\theta\theta}$ are 0.93×10^6 (mm^{-1}) and -0.92×10^{-10} (N mm/mm), respectively, at the top; 0.8×10^6 (mm^{-1}) and -0.79×10^{-10} (N mm/mm), respectively, at the bottom, and -1.04×10^6 (mm^{-1}) and 1.03×10^{-10} (N mm/mm), respectively, in the sides. The most flattened cross section is in the middle of the kink (Fig. 6b) where the top side of the kink even slightly displaces inwards. The longitudinal curvature k_{zz} is almost zero at all sections along the kink.

The curvatures and the bending moments were compared with the results from the Vodenitcharova-Zhang model [6] and it was found that in the middle of the kink $M_{\theta\theta}$ is 1.49×10^{-10} (N mm/mm) in the top wall and 1.52×10^{-10} (N mm/mm) in the side walls. Obviously, these values are close to the results from MD (Fig. 6b). However, the Vodenitcharova-Zhang model underestimates $M_{\theta\theta}$ at the bottom wall, where it is 0.4×10^{-10} (N mm/mm) in the middle of the kink. Nevertheless, the contribution of such moment to the energy of the SWNT is small.

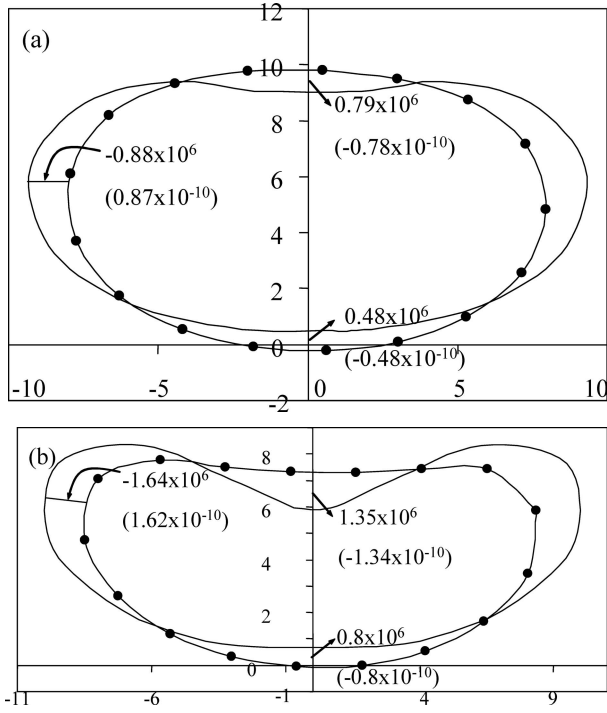


Figure 6 (a) Deformed cross section (line with solid circles, where the circles represent the atoms) and the diagram of $k_{\theta\theta}/M_{\theta\theta}$ (solid line) at a distance of R from the middle of the kink, $\psi = 28^\circ$. The figures outside the brackets are the values of $k_{\theta\theta}$ (in mm^{-1}) and the figures in the brackets are the values of $M_{\theta\theta}$ (in N mm/mm); the cross-sectional dimensions are in \AA ; (b) Deformed cross section (line with solid circles, where the circles represent the atoms) and the diagram of $k_{\theta\theta}/M_{\theta\theta}$ (solid line) in the middle of the kink at $\psi = 28^\circ$. The figures outside the brackets are the values of $k_{\theta\theta}$ (in mm^{-1}) and the figures in the brackets are the values of $M_{\theta\theta}$ (in N mm/mm). The cross-sectional dimensions are in \AA .

Similar considerations can be given to the kink development at a bending angle of $\psi = 64^\circ$. The length of the kink l can be determined from the longitudinal view (Fig. 7a) and appears to be around $3R$. At the ends of the kink, the SWNT is inclined at $\psi = 32^\circ$. Along the kink, within a length of $2l$ from the middle of the kink, the bottom line at $X' = 0$ resembles an arc with a radius of 65.45\AA . The top of the kink consists of two zones. Zone 1 contains two almost triangular areas between the kink's ends and sections at a distance of $1.69R$ from the middle of the kink. Zone 2 is between these sections and the middle of the kink, where the longitudinal lines in the top part of the kink are curvilinear. The line in Zone 2 having $X' = 0$ is almost circular at $Z' = 0$ and has a radius $R' = 20.35 \text{\AA}$; so that its longitudinal curvature is $k_{zz} = -1/R' = -4.91 \times 10^5 \text{ mm}^{-1}$. The bottom of the kink in Zone 2 is slightly curved and the fibre $X' = 0$ resembles a circular arc having $R' = 65.45 \text{\AA}$; therefore its longitudinal curvature k_{zz} is $-1/R' = -1.53 \times 10^5 \text{ mm}^{-1}$.

It is observable that the shape of the deformed cross sections of the kink at large angles differs from those at small angles, (Fig. 7b). Even at the ends of the SWNT, the cross section is no longer circular but oval having $\zeta = 0.094$. At a distance of $3R$ from the middle of the kink, the cross section is also oval experiencing a drop from the

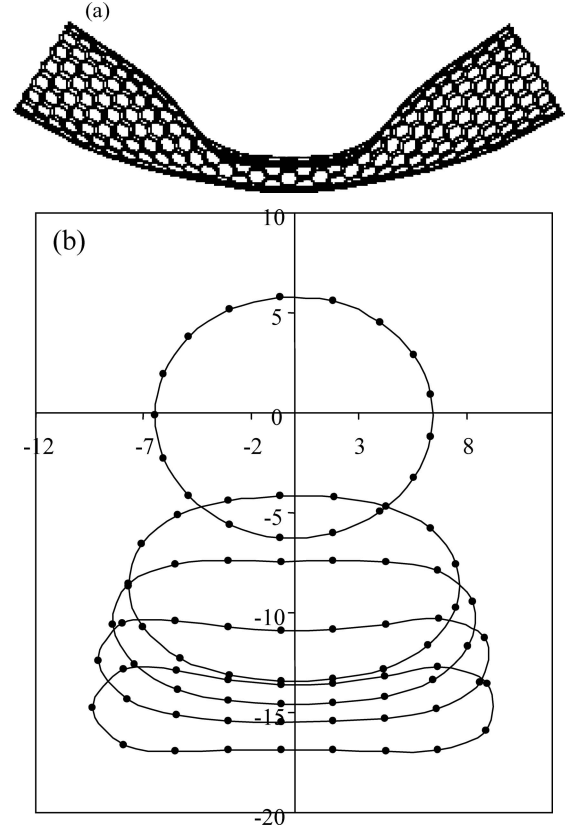


Figure 7 (a) Longitudinal section of the SWNT showing the kink formed at $\psi = 64^\circ$; (b) Cross-sectional view A-A of (a) of the deformed atomic rings at a bending angle of $\psi = 64^\circ$, where the solid circles represent the atoms.

original circular shape $\delta = 4.08 \text{\AA}$; the minimum distance between the top wall and the bottom wall is 9.24\AA and ζ is 0.306.

Towards the middle of the kink, the cross section becomes more deformed. At a distance of $1.69R$ from the middle of the kink, the cross section is similar to the one at the middle of the kink. The drop in cross section, δ , is 8.74\AA , the minimum distance between the top and bottom walls is 4.57\AA , and the flattening ratio ζ is 0.657. The curvatures and the bending moments increase accordingly; at the top of the cross section $k_{\theta\theta}$ and $M_{\theta\theta}$ are $1.37 \times 10^6 \text{ (mm}^{-1}\text{)}$ and $-1.36 \times 10^{-10} \text{ (N mm/mm)}$, respectively; at the bottom of the cross section $1.183 \times 10^6 \text{ (mm}^{-1}\text{)}$ and $-1.172 \times 10^{-10} \text{ (N mm/mm)}$, respectively; and in the sides $-2.285 \times 10^6 \text{ (mm}^{-1}\text{)}$ and $2.264 \times 10^{-10} \text{ (N mm/mm)}$, respectively. Obviously the sides bulge significantly resembling a circular arc with a radius of 2.64\AA .

At the middle of the kink, the cross section of the SWNT becomes almost fully collapsed. Both the top and bottom parts flatten, even bend inwards; the distance between them was measured to be 3.21\AA , which is close to the equilibrium distance between two graphite sheets of 3.4\AA . It was also calculated that $\delta = 10.1 \text{\AA}$ and $\zeta = 0.76$. The circumferential curvatures and bending moments were calculated as well shown in Figs. 8a and b, where the results at $\psi = 28^\circ$ are also given for comparison (note

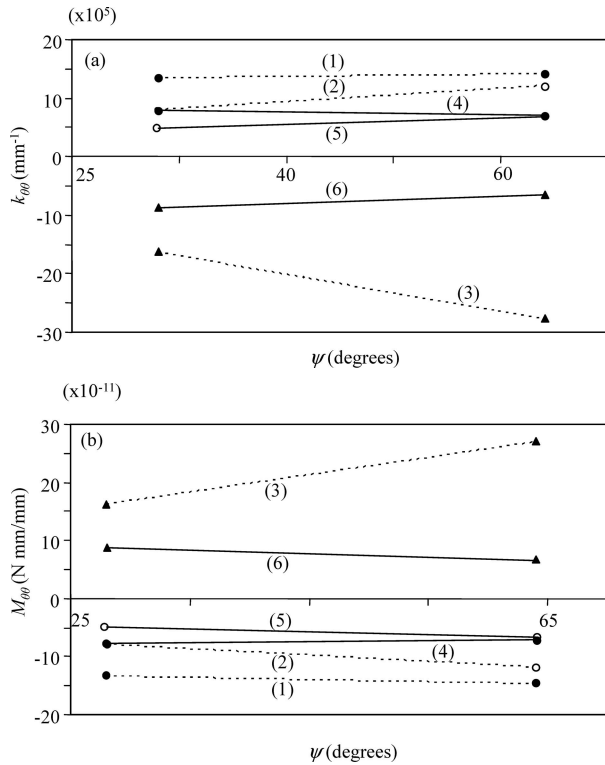


Figure 8 (a) Circumferential curvature, $k_{\theta\theta}$, at various points of the cross section at the end of the kink (solid lines) and in the middle of the kink (dotted lines), vs. the total bending angle ψ : (1) $k_{\theta\theta}$ at the top of the cross section in the middle of the kink, (2) $k_{\theta\theta}$ at the bottom of the cross section in the middle of the kink, (3) $k_{\theta\theta}$ at the sides of the cross section in the middle of the kink, (4) $k_{\theta\theta}$ at the top of the cross section at the end of the kink, (5) $k_{\theta\theta}$ at the bottom of the cross section at the end of the kink, (6) $k_{\theta\theta}$ at the sides of the cross section at the end of the kink; (b) Circumferential moment, $M_{\theta\theta}$, at various points of the cross section at the end of the kink (solid lines) and in the middle of the kink (dotted lines), vs. the total bending angle ψ : (1) $M_{\theta\theta}$ at the top of the cross section in the middle of the kink, (2) $M_{\theta\theta}$ at the bottom of the cross section in the middle of the kink, (3) $M_{\theta\theta}$ at the sides of the cross section in the middle of the kink, (4) $M_{\theta\theta}$ at the top of the cross section at the end of the kink, (5) $M_{\theta\theta}$ at the bottom of the cross section at the end of the kink, (6) $M_{\theta\theta}$ at the sides of the cross section at the end of the kink.

that the length of the kink is $l = R$ for $\psi = 28^\circ$ and $l = 3R$ for $\psi = 64^\circ$). It is evident that $k_{\theta\theta}$ and $M_{\theta\theta}$ at the top and bottom parts of the cross sections do not vary much with the bending angle, ψ . However, the sides of the nan-

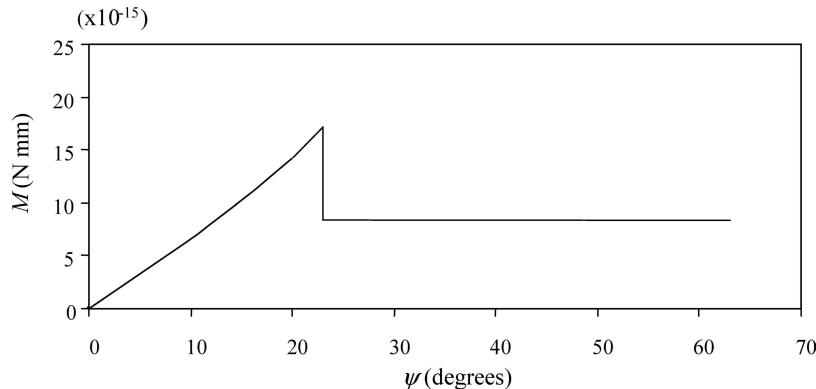


Figure 9 Bending moment M vs. bending angle.

otube bulge outwards significantly and have an almost constant circumferential curvature $k_{\theta\theta}$ of $-2.78 \times 10^6 \text{ (mm}^{-1}\text{)}$, which corresponds to a circular arc of a radius 2.33\AA . When applied to this bending angle ($\psi = 64^\circ$), the Vodenitcharova-Zhang model provides close results: $M_{\theta\theta} = 1.49 \times 10^{-10} \text{ (N mm/mm)}$ in the top wall and $2.13 \times 10^{-10} \text{ (N mm/mm)}$ in the sides. A similar note can be made as in the case of $\psi = 28^\circ$, that the Vodenitcharova-Zhang model underestimates $M_{\theta\theta}$ at the bottom wall, where it is $0.7 \times 10^{-10} \text{ (N mm/mm)}$. The longitudinal curvatures are small; line $X' = 0$ has $k_{zz} = 4.91 \times 10^5 \text{ mm}^{-1}$ in the top wall and $k_{zz} = 1.53 \times 10^5 \text{ mm}^{-1}$ in the bottom wall.

5. Bending capacity of the SWNT in pure bending

Rotating the ends of the SWNT will induce pure bending since each cross section will only turn about an axis parallel to the X-axis and passing through the centroid of the cross section. The other internal forces will be zero. The magnitude of the bending moment M is calculated from the strain energy graph (Fig. 1) as $(\partial U / \partial \psi)$.

The variation of M with the bending angle ψ is plotted in Fig. 9; M is almost linear in the pre-buckling zone, has a drop at the point of local buckling and is almost constant in the post-buckling zone. Obviously, the kink formation decreases the bending capacity of the nanotube.

6. Conclusions

This paper examines in detail the deformation mechanism of a SWNT, using MD analysis in conjunction with the continuum mechanics. It was found that the SWNT buckles locally at a critical bending angle, and consequently kinks upon further loading. The phenomenon of kinking is associated with the formation of moving hinge lines located in the side walls of the kink, and one stationary hinge line located in the top wall in the middle of the kink. The bending capacity of the SWNT has also been estimated for the pre-buckling and post-buckling regimes. It was found that at small angles the simplified mechanics model [6] predicts well the point of local buckling, the kink parameters, the bending moments in the walls of the

SWNT and the bending moment M applied at the end sections of the beam.

Acknowledgement

This work was supported by an ARC Discovery Grant.

References

1. D. SRIVASTAVA, *et al.*, *J. Phys. Chem. B* **103** (1999) 4330.
2. S. IJJIMA, *J. Chem. Phys.* **104** (1996) 2089.
3. H. W. C. POSTMA, *et al.*, *Adv. Mater.* **12** (2000) 1299.
4. M. R. FALVO, *et al.*, *Nature*. **389** (1997) 582.
5. B. I. YAKOBSON, *et al.*, *Phys. Rev. Lett.* **76** (1996) 2511.
6. T. VODENITCHAROVA and L. C. ZHANG, *Phys. Rev.* **B69** (2004) 115410.
7. K. MYLVAGANAM and L. C. ZHANG, *Carbon* **42** (2004) 2025.
8. D. W. BRENNER, *Phys. Rev.* **B42** (1990) 9458.
9. D. W. BRENNER, *et al.*, *J Phys. Cond. Matter* **14** (2002) 783.
10. C. R. CALLADINE, "Theory of Shell Structures" (Cambridge University Press, 1983).
11. T. VODENITCHAROVA and L. C. ZHANG, *Phys. Rev.* **B68** (2003) 165401.

*Received 4 January
and accepted 18 July 2005*